

Bifocal-Lens Antenna Based OAM Communications System

Shanghua Gao, Wenchi Cheng, *Senior Member, IEEE*, Wei Zhang, *Fellow, IEEE*, and Hailin Zhang, *Member, IEEE*

E-mail: {shgao@stu.xidian.edu.cn, wccheng@xidian.edu.cn, w.zhang@unsw.edu.au, hlzhang@xidian.edu.cn}

Abstract—Orbital angular momentum (OAM) based radio vortex wireless communications have received much attention recently because it can significantly increase the spectrum efficiency. The uniform circular array (UCA) is a simple antenna structure for high spectrum efficiency radio vortex wireless communications. However, the OAM based electromagnetic waves are vortically hollow and divergent, which may result in the signal loss. Moreover, the divergence of corresponding OAM based electromagnetic wave increases as the order of OAM-mode and radius of UCA increases. Therefore, it is difficult to use high-order OAM-mode, because the corresponding received signal-to-noise ratio (SNR) is very small. To overcome the difficulty of high-order OAM modes transmission, in this paper we propose a lens antenna based electromagnetic waves converging scheme, which maintains the angular identification of multiple OAM-modes for radio vortex wireless communications. We further develop a bifocal lens antenna to not only converge the electromagnetic wave, but also compensate the SNR loss on traditional electromagnetic waves. Simulation results show that the proposed bifocal lens can converge the OAM waves into cylinder-like beams, providing an efficient way to increase the spectrum efficiency of wireless communications.

Index Terms—Orbital angular momentum (OAM), bifocal lens antenna, convergence, uniform circular array (UCA), wireless communications, spectrum efficiency.

I. INTRODUCTION

DUE to the rapid development of wireless communications, it is now very crowded within the available radio spectrum. Traditionally, the wireless communication was built on the linear momentum based plane-electromagnetic (PE) wave [2], [3]. However, PE wave has not only the linear momentum, but also the orbital angular momentum (OAM), which is the result of a signal possessing helical phase fronts. The OAM-based radio vortex waves can support multiple orthogonal states/modes, which can be utilized to significantly increase the spectrum efficiency (SE) of wireless communications [4], [5], [6], [7], [8].

There exist a number of antenna structures to generate OAM-based radio vortex beams. A design of flat-lensed spiral phase plate (SPP) was proposed to generate OAM beams [9], [10]. The impedance-matched reflectivity SPP improved the

reflectivity of SPP by more than 20 dB [11]. The authors of [12] proposed a parabolic reflecting antenna with an azimuthally deformed Cassegrain subreflector to generate arbitrary OAM-modes. However, these schemes cannot simultaneously generate multiple OAM beams with different OAM-modes. In order to increase SE of wireless communications, multiple OAM-modes need to be generated and transmitted within the same frequency band at the same time. The uniform circular array (UCA), through changing the phase difference of feeds [13], is an effective antenna structure to generate multiple OAM-modes within the same frequency band at the same time [14], [15], [16], [17].

Recently, it was shown that the electromagnetic (EM) wave with UCA generated OAM are vortically hollow and divergent [12]. Moreover, the EM wave becomes more and more divergent as the order of OAM-mode increases [18], which leads to very low received signal-to-noise ratio (SNR) for high-order OAM waves [19]. Although, the divergent angle decreases as the radius of UCA increases, it is not practical to greatly increase the radius of UCA. In order to facilitate the radio vortex wireless communications, it is desirable to control the OAM beams into a small radiation range. The SPP can generate converged single mode OAM beam [20] while the multi-layer amplitude-phase-modulated surfaces can transform a quasi-spherical wave into non-diffractive single mode OAM beam [21]. However, to the best of our knowledge, no effective method has been proposed to generate multiple simultaneous converged OAM beams. In this work, we focus on the study of generating multiple OAM beams with different OAM-modes while maintaining a small divergent angle all OAM-modes.

In fact, the lens has the ability of convergence [22], which can be used for converging OAM beams. In addition, the lens has no inherent frequency bandwidth limitation, which can be easily extended to many kinds of application scenarios. In this paper, we propose to use the UCA and lens-based antenna to converge multiple modes OAM beams. To avoid the severe loss of the strength of PE beams and OAM beams with low-order OAM-mode due to the large thickness in the center of the lens, we propose a bifocal lens, which has the internal and external parts with different focal distance. In addition, the internal lens has a longer focal distance than the external lens, mitigating the SNR downgrading for PE wave, i.e., OAM wave with mode 0. The converged beams maintain the original wavefront angles. Conventional lens reduces the loss by changing the thickness of the lens. It ensures the

Part of this work has been accepted by the IEEE/CIC International Conference on Communications in China (ICCC), Qingdao, China, 2017 [1].

Shanghua Gao, Wenchi Cheng, and Hailin Zhang are with the State Key Laboratory of Integrated Services Networks, Xidian University, Xi'an, 710071, China.

Wei Zhang is with the University of New South Wales, Sydney, Australia.

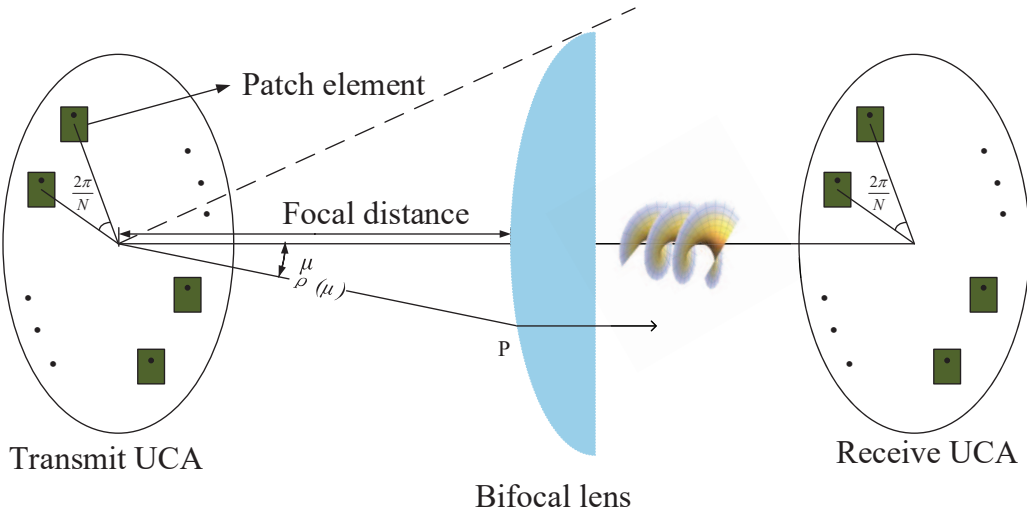


Fig. 1. The lens-assisted radio vortex wireless communications model.

refraction direction of PE wave remains the same [22]. Due to the diversity of OAM divergence angles, we use a novel strategy which uses different focal distances for OAM beams with different OAM-modes.

Our contributions can be summarized as follows:

- (1) We reveal that the divergence angle of OAM beams is related to the radius of UCA. Besides, we give the relationships between the radius of UCA and the divergence angle of OAM beams.
- (2) We show that the lens doesn't change the wavefront angle of OAM beams, which is very crucial for orthogonal multiplexing in wireless communications.
- (3) We propose the bifocal lens to not only converge OAM beams but also compensate the SNR loss on PE waves and low-order OAM beams.

The rest of this paper is organized as follows. Section II describes the system model of lens-assisted converged radio vortex wireless communications. Section III, and IV, and V design and analyze UCA antenna, lens antenna, and bifocal lens antenna, respectively. We also show the lens antenna does not change the wavefront of OAM beams. Section VI evaluates our developed lens converging and the spectrum efficiency enhancement. The paper concludes with Section VII.

II. THE SYSTEM MODEL

We consider the lens-assisted radio vortex wireless communications model, as shown in Fig. 1, where the transmitter and receiver are both UCA antennas with N array-elements equally distributed on the circle. By controlling the phase information, UCA with N elements is designed to simultaneously generate multiple OAM beams with different OAM-modes. The phase information of adjacent element is linearly increased by $2\pi l/N$, where l is the index/order of OAM-mode. The maximum index of OAM-mode that UCA can support is limited by $-N/2 \leq l < N/2$ [10]. The PE beam (OAM wave with mode 0) is generated when all elements of UCA have the same phase information. The UCA generated

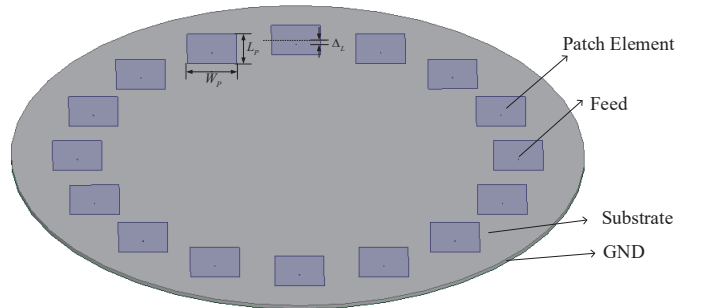


Fig. 2. The profile of 16 patch elements UCA with 16 patch elements.

OAM waves are vortically hollow and divergent, depending on the radius of UCA and the index of OAM-mode [18]. The lens antenna is designed based on the principle of wave path consistency [22]. The OAM beams can be treated as emitting from the central point of the transmit UCA. We place the UCA at the focal point of lens antenna. Multiple divergent OAM beams generated by UCA are sent to lens antenna, where P is the incident point the beam entered the lens, and μ is the angle between the beam transmitting direction and the central axis. Lens antenna converges these OAM beams into cylinder-like beams while maintaining the original wavefront of each OAM-mode. Therefore, the receive antenna can efficiently receive the OAM beams within a small reception area.

III. ANALYSIS OF UNCONVERGED OAM BEAMS

In this section, we design and analyze the UCA antenna. We analyze the divergence angle of OAM beams. We reveal that the divergence angle of OAM beams is related to the radius of UCA. Also, we give the relationships between the radius of UCA and the divergence angle of OAM beams. We then derive the capacity for OAM based radio vortex wireless communications with unconverged OAM beams.

A. Design of UCA Antenna

We design the patch based UCA antenna. The profile of a 16 patch elements based UCA is shown in Fig. 2, where patch elements are equally distributed around the circle. To achieve the best feed performance, it is needed to design the size of patch elements [23]. For the specific design of UCA antenna, please refer to the APPENDIX of this paper.

B. Characteristics of OAM Based Vortex Beams

According to [24], the E field of OAM beams can be expressed as follows:

$$E(r, \theta, \varphi) = A(r)e^{il\varphi}J_l(2kR\sin\theta), \quad (1)$$

where r represents the distance between beams and axis, φ is azimuth, l is the index of OAM-mode, $J_l(\cdot)$ is Bessel function, θ is the angle between the normal to the plane of the circle and the direction from UCA to the field, and $A(r)$ is the amplitude of OAM beams. R is the radius of UCA, which is the distance from the center of transmit UCA to the center of patch elements. The phase rotation $\exp(il\varphi)$ controls the spatial distribution of OAM beam. The expression for $A(r)$ can be given as follows [24]:

$$A(r) = -j\frac{\mu_0\omega d}{4\pi}Nj^{-l}\frac{e^{ikr}}{r}, \quad (2)$$

where j represents the current density of the electric dipole, ω is wavelength, $k = \omega/c$, μ_0 is the magnetic conductivity, and d is the length of electric dipole.

We denote by θ_l the divergent angle of the l th OAM-mode, where the corresponding OAM beam has the largest gain. We notice that the number of patch elements causes little impact on the divergent angle θ_l . By simulating using HFSS [25], we get the relationship between R and θ , as shown in Table I. θ_l decreases as R increases, while the descent rate of θ_l decreases as R increases. Also, θ_l increases as OAM-mode increases. Analyzing the obtained data in Table I, we propose the following two mathematical models to characterize the relationship between R and θ_l .

Model 1: The first model is given as follows:

$$\theta_l = a_l R^{b_l}, \quad (3)$$

where a_l is the factor that controls the magnitude of θ_l , while b_l is the factor that controls the descent rate of curves. To accommodate the descent rate, b_l should be a negative number.

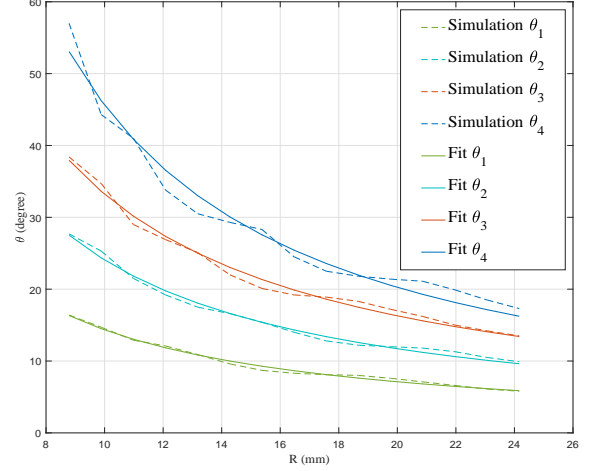
Model 2: The second model is given as follows:

$$\theta_l = \frac{p_l}{(R+q_l)}, \quad (4)$$

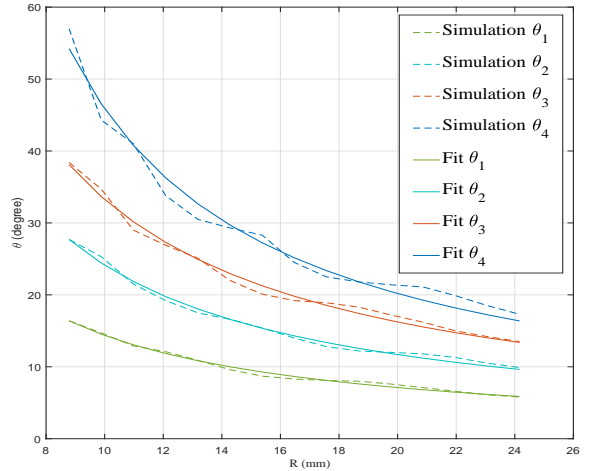
where p_l mainly controls the the magnitude of θ_l and q_l controls is a negative number controlling the descent rate of curves.

Figure 3 gives the relationship between the radius of UCA and the divergent angle of OAM beams. The curves in Fig. 3(a) indicate the relationship between θ_l and R is in the form of $\theta_l = a_l R^{b_l}$. The curves in Fig. 3(b) are in the form of $\theta_l = \frac{p_l}{(R+q_l)}$. The specific values of a_l, b_l, p_l , and q_l that obtained

by simulation is shown in Table. II. As shown in Fig. 3, our proposed two curves can fit the relationship between θ_l and R quite well. The divergent angle increases as the increase of OAM-mode. In addition, the slope of divergent angle decreases as the radius of UCA increases.



(a) $\theta_l = a_l R^{b_l}$



(b) $\theta_l = \frac{p_l}{(R+q_l)}$

Fig. 3. The relationship between the radius of UCA and the divergent angle of OAM beams.

C. Capacity analysis of OAM Based Radio Vortex Wireless Communications

The received power of receive antenna, denoted by P_r , can be given as follows: [26]:

$$P_r = \frac{G_t A_{er}}{4\pi d^2} P_t, \quad (5)$$

where P_t is the power of transmit antenna, G_t is the gain of transmit antenna, d represents the distance between the receive antenna and transmit antenna, and A_{er} represents the effective

TABLE I
THE SIMULATED RELATIONSHIP BETWEEN THE RADIUS OF UCA AND THE DIVERGENT ANGLE OF OAM BEAMS.

R (mm)	8.8	9.9	11.0	12.1	13.2	14.3	15.4	16.5	17.6	18.7	19.8	20.9	22.0	23.1	24.2
θ_1 (degree)	16.4	14.7	12.9	12.1	10.9	9.6	8.7	8.3	8.1	8	7.6	7.1	6.6	6.1	5.8
θ_2 (degree)	27.7	25.3	21.5	19.2	17.5	16.6	15.4	14	12.8	12.2	12	11.8	11.3	10.5	9.9
θ_3 (degree)	38.4	34.7	29	26.9	25.1	22	20.1	19.2	18.9	18.3	17.2	16.2	15	14.2	13.5
θ_4 (degree)	57	44.3	41	33.8	30.5	29.3	28.3	24.5	22.5	21.8	21.4	21.1	19.9	18.5	17.3

TABLE II
SPECIFIC VALUES OF a_l, b_l, p_l AND q_l .

OAM-mode	a_l	b_l	p_l	q_l
1	147	-1.011	140.9	-0.1902
2	263.2	-1.039	227.2	-0.5844
3	354.3	-1.028	317.1	-0.4647
4	676.3	-1.171	360.7	-2.135

reception area when the antenna is pointed to the maximum direction of the beam. We assume that the radius of receive antenna is constant, denoted by r_0 , and the transmit antenna is aligned with the receive antenna. The effective reception area of the receive antenna can be written as follows:

$$A_{er} = \frac{\lambda^2 G_0}{4\pi}, \quad (6)$$

where G_0 is the gain of receive antenna.

For OAM beams, each diverged OAM beam has a divergent angle with the value of $2\theta_l \pm 2\Delta\theta_l$, where $\Delta\theta_l$ is the half-power beamwidth of the OAM beam corresponding to the l th mode. Since the effective reception area depends on the propagation distances, we discuss the following three cases.

Case 1: The receive antenna covers the outside of the half-power beam $2\theta_l + 2\Delta\theta_l$ when the power of main lobe can be fully received. The corresponding SNR and the region of d are given as follows:

$$\begin{cases} \text{SNR}_l = \frac{P_r}{N_0} = \frac{G_t(l)A_{er}}{(4\pi d)^2 N_0} P_t = \frac{G_t(l)\lambda^2 G_0}{(4\pi d)^2 N_0} P_t; \\ d < \frac{r_0}{\tan(\theta_l + \Delta\theta_l)}, \end{cases} \quad (7)$$

where $G_t(l)$ is the gain when the transmit antenna emits the l th OAM-mode.

Case 2: The receive antenna cannot cover the inside of the half-power beam $2\theta_l - 2\Delta\theta_l$ when the power of main lobe cannot be received. In this case, we have $P_r = 0$ and thus we have

$$\begin{cases} \text{SNR}_l = 0; \\ d > \frac{r_0}{\tan(\theta_l - \Delta\theta_l)}. \end{cases} \quad (8)$$

Case 3: The receive antenna partially receives the beams. We denote by $G_t(l, \theta)$ the maximum power of the l th mode OAM beams that can be received from the direction of θ . Under this scenario, the SNR and the region of d can be obtained as follows:

$$\begin{cases} \text{SNR}_l = \frac{P_r}{N_0} = \frac{G_t(l, \theta)A_{er}}{(4\pi d)^2 N_0} P_t = \frac{G_t(l, \theta)\lambda^2 G_0}{(4\pi d)^2 N_0} P_t; \\ \frac{r_0}{\tan(\theta_l + \Delta\theta_l)} < d < \frac{r_0}{\tan(\theta_l - \Delta\theta_l)}. \end{cases} \quad (9)$$

Now, we can derive the capacity of the OAM based radio vortex wireless communications using divergent OAM beams indexed from 1 to L [27], denoted by C , in Eq. (10). SNR_l is the SNR of radio vortex wireless communication using the l th divergent OAM-mode and B is system bandwidth. In case 1, when the propagation distance is short, the main lobe of unconverged beams can be fully received. In case 2, when the propagation distance is relatively long, the main lobe of beams can only be partly received. Thus, the capacity decreases faster. In case 3, when the propagation distance is very large, the beams cannot be received by the antenna. Thus, the obtained capacity is very close to 0. Since multiple OAM-modes can be utilized together, the capacity increases as more and more OAM-modes (especially the high-order OAM-modes) are used. Because F_r and λ are in reciprocal relationship. The operating frequency is also related to the effective reception area of receiving antenna, the capacity increases as operating frequency increases.

IV. ANALYSIS OF LENS ANTENNA

In this section, we design and analyze the lens antenna. We analyze the phase and amplitude of OAM beams converged by the lens. We show that the lens doesn't change the wavefront angle of OAM beams, which is very crucial for orthogonal multiplexing in wireless communications. We then derive the capacity of lens-converged OAM based radio vortex wireless communications.

A. Design of Lens Antenna

According to Fermat's principle, the wave path from the UCA through the lens to the aperture plane needs to be equalized [23]. The wave path along the axis and the wave path at any angle denoted as μ are equal when reaching the aperture plane of the lens, as shown in Fig. 1. The lensmaker's equation in polar coordinates is given as follows [28], [29]:

$$\rho(\mu) = \frac{(n-1)f}{n \cos \mu - 1}, \quad (11)$$

where f represents the focal distance, $n = \sqrt{\varepsilon_r \mu_r}$ is the index of refraction with ε_r and μ_r representing the relative permittivity and permeability of the lens medium, respectively.

Substituting $\rho(\mu)^2 = (x+f)^2 + y^2$ and $\rho(\mu) = f + nx$ into Eq. (11), the lensmaker's equation in cartesian coordinates can be derived as follows:

$$(n^2 - 1)x^2 + 2(n-1)fx - y^2 = 0, \quad (12)$$

where (x, y) is the coordinates of point P . It can be seen that the lensmaker's equation is hyperbolic with a progressive line.

$$C = \sum_{l=1}^L B \log_2(1 + \text{SNR}_l) = \begin{cases} \sum_{l=1}^L B \log_2 \left(1 + \frac{G_t(l) \lambda^2 G_0 P_t}{(4\pi d)^2 N_0} \right) & d < \frac{r_0}{\tan(\theta_l + \Delta\theta_l)}; \\ \sum_{l=1}^L B \log_2 \left(1 + \frac{G_t(l, \theta) \lambda^2 G_0 P_t}{(4\pi d)^2 N_0} \right) & \frac{r_0}{\tan(\theta_l + \Delta\theta_l)} < d < \frac{r_0}{\tan(\theta_l - \Delta\theta_l)}; \\ 0 & d > \frac{r_0}{\tan(\theta_l - \Delta\theta_l)}. \end{cases} \quad (10)$$

Thus, the maximum divergent angle that the lens antenna can support can be obtained as follows:

$$\mu_{\max} = \arccos \frac{1}{n}. \quad (13)$$

This angle can be used to verify whether the designed lens antenna covers the divergent angle of OAM beams or not. We denote by θ_{\max} the maximum divergent angle of OAM beams. Thus, we have $\theta_{\max} < \mu_{\max}$. Then, the diameter, denoted by D , for the lens antenna can be derived as follows:

$$D = 2\rho(\mu) \sin \theta_{\max} = \frac{2(n-1)f \sin \theta_{\max}}{n \cos \theta_{\max} - 1}. \quad (14)$$

Moreover, in order to limit the lens size while maintaining a low downgrading, we need to design the values of D and f . We denote by m the coefficient that balances D and f . Then, we have

$$D = mf. \quad (15)$$

Combining Eq. (14) and Eq. (15), we can obtain m as follows:

$$m = \frac{2(n-1) \sin \theta_{\max}}{n \cos \theta_{\max} - 1}. \quad (16)$$

For Model 1 and Model 2 corresponding to Eqs. (3) and (4), respectively, m can be re-written as:

$$m = \frac{2(n-1) \sin(a_j R^{b_j})}{n \cos(a_j R^{b_j}) - 1}, \quad (17)$$

and

$$m = \frac{2(n-1) \sin \left[\frac{p_j}{(R+q_j)} \right]}{n \cos \left[\frac{p_j}{(R+q_j)} \right] - 1}, \quad (18)$$

respectively.

Next, we show that converging does not change the wavefront of OAM beams. We give the relationships between the phase change of beam and its passing wave path as follows [30]:

$$\Delta\varphi(r) = kL(r), \quad (19)$$

where $r^2 = x^2 + y^2$ and $L(r)$ is the wave path.

Observing Eq. (19), we find that the beam passing through the lens causes phase changes and the lens has a phase modulation for the incident wave. Because the design of the lens antenna uses the wave path consistent principle, the wave path $L(r)$ between transmit UCA and lens antenna's aperture plane is constant regardless of the variation of r . We denote by ΔL_p the wave path. Ignoring the impact of the lens on the amplitude of incident wave and combining Eq. (1), the E field

of OAM beams after passing through the lens antenna can be derived as follows:

$$\begin{aligned} E'(r, \theta, \varphi) &= A(r) J_l(2kR \sin \theta) e^{il\varphi + i\Delta\varphi(r)} \\ &= A(r) J_l(2kR \sin \theta) e^{il\varphi + ik\Delta L_p} \\ &= e^{ik\Delta L_p} A(r) J_l(2kR \sin \theta) e^{il\varphi}. \end{aligned} \quad (20)$$

Therefore, after passing through the lens antenna, the phases of OAM wave corresponding to different angles only increased by a fixed value $\Delta\varphi$. Thus, our designed lens antenna maintains the wavefront characteristics of OAM beams while converging the OAM beams into cylinder-like waves.

The lens changes the amplitude distribution of beams on the antenna aperture surface [29]. The feed power is equal to the caliber power in the ideal scenario. However, due to the divergence of OAM beams, there exists power loss since the size of lens is limited. The amplitude of beams after passing through the lens, denoted by $A'_L(r, f)$, is given as follows:

$$A'_L(r, f) = A(r) \frac{a(n \cos \varphi - 1)^3}{f^2(n-1)^2(n - \cos \varphi)}, \quad (21)$$

where a is the ratio of the energy entering the lens to the total energy. In addition, the downgrading caused by the lens is proportional to the thickness of the lens. The amplitude of beams after passing through the lens, denoted by $A_L(r, f)$ can be written as [31]:

$$A_L(r, f) = A'_L(r, f) - pT(f, \theta), \quad (22)$$

where p is the downgrading factor related to material of lens given range $1 \sim 10$ [22] and $T(f)$ is the thinness of lens given as follows:

$$T(f, \theta) = -\frac{f}{n+1} + \sqrt{\left(\frac{f}{n+1}\right)^2 + \frac{\left(\frac{D}{2} - f \tan \theta\right)^2}{n^2 - 1}}. \quad (23)$$

B. Capacity analysis of lens-converged OAM Based Radio Vortex Wireless Communications

After converging, OAM beams are almost converged into cylinder-like beam. However, the converged OAM beams still have the small divergent angle, denoted by σ . By substituting Eq. (21) into Eq. (7), the maximum propagation distance of beams, denoted by d_{\max} , and SNR of lens based radio vortex wireless communication using converged OAM with the index l , denoted by SNR'_l can be written as follows:

$$\begin{cases} \text{SNR}'_l = \frac{\left[G'_t(l) \frac{a(n \cos \varphi - 1)^3}{f^2(n-1)^2(n - \cos \varphi)} - pT(f, \theta_l) \right] A_{er}}{(4\pi d)^2 N_0} P_t \\ \quad = \frac{\left[G'_t(l) \frac{a(n \cos \varphi - 1)^3}{f^2(n-1)^2(n - \cos \varphi)} - pT(f, \theta_l) \right] \lambda^2 G_0}{(4\pi d)^2 N_0} P_t; \\ d_{\max} = \frac{r_0}{\tan \sigma}, \end{cases} \quad (24)$$

$$C_L = \sum_{l=1}^L B \log_2 (1 + \text{SNR}'_l) = \sum_{l=1}^L B \log_2 \left\{ 1 + \frac{\left[G'_t(l) \frac{a(n \cos \varphi - 1)^3}{f_0^2 (n-1)^2 (n - \cos \varphi)} - pT(f, \theta_l) \right] \lambda^2 G_0}{(4\pi d)^2 N_0} P_t \right\}. \quad (25)$$

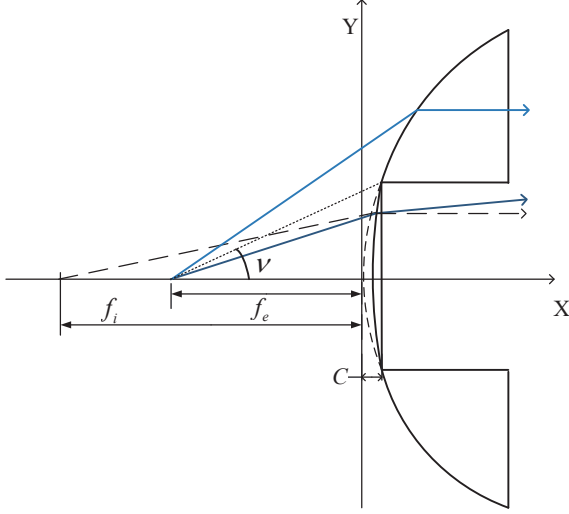


Fig. 4. Schematic diagram of bifocal lens antenna.

where $G'_t(l)$ is the gain when the transmit antenna (including the UCA antenna and the lens antenna) emits the converged l th mode OAM beams.

The capacity of converged OAM beams can be written in Eq. (25), where C_L is capacity of radio vortex wireless communication using converged OAM with the index from 0 to L .

V. ANALYSIS OF BIFOCAL LENS ANTENNA

In this section, we design and analyze the bifocal lens antenna. We propose the bifocal lens to not only converge OAM beams, but also compensate the SNR loss on PE waves and low-order OAM beams. We then derive the capacity of bifocal lens OAM based radio vortex wireless communications.

A. Design of Bifocal Lens Antenna

Since the center of lens antenna is thicker than other parts, the strength of PE beam (i.e., OAM beam with mode 0) and OAM beams with low-order OAM-mode severely downgrades after passing through the lens according to Eq. (22). To solve this problem, we design the bifocal lens antenna, as shown in Fig. 4, which is divided into the internal and external parts with different focal distances. The internal lens has a long focal distance while the external lens has a short focal distance. Thus, the bifocal lens can be thinner than the single focal lens in the center area, significantly mitigating the SNR downgrading of PE beam and OAM beams with low-order OAM-mode.

We denote by ν the angle corresponding to the boundary of separating the internal lens and the external lens. Since each

OAM-mode has an inherent divergent angle of θ_l , where the amplitude corresponding to the l th OAM-mode has the largest value. To avoid two parts of lens causing different convergence effects on the same OAM-mode, ν should be selected in the middle of different divergent angles. The internal lens and the external lens share the same spindle. Based on the lensmaker's equation of single focal lens antenna in Eq. (12), we can write the lensmaker's equation for bifocal lens antenna as follows:

$$\begin{cases} (n^2 - 1)(z - C)^2 + 2(n - 1)f_i \times (z - C) - x^2 = 0; \\ (n^2 - 1)z^2 + 2(n - 1)f_e \times z - x^2 = 0; \\ \frac{x}{z + f_e} = \tan \nu; \\ \theta_l < \nu < \theta_{l+1}, \end{cases} \quad (26)$$

where f_i and f_e represent the focal distances of the internal lens and external lens, respectively. Solving Eq. (26), we can obtain the boundary's coordinates of the internal lens and the external lens. In our design, f_e is a prefixed value. We need to obtain the value of f_i to solve Eq. (26). The parameter that controls the thickness of the internal lens and impacts the convergence, denoted by ρ , is written as follows:

$$f_i = \rho f_e, \quad (27)$$

where $\rho > 1$.

To obtain ρ , we need to make sure that the internal lens has the similar convergence effect compared with the external lens. Fig. 5 shows the refraction path of internal lens, where the solid line indicates the path of OAM beams that emitted from focal f_e . In the range of the internal lens, due to the relatively long focal distance of the internal lens, OAM beams still have a small divergent angle, denoted by τ , after passing through the lens, which can be easily obtained by Fig. 5:

$$\tau = \arcsin \left[\frac{1}{n} \sin(\theta_l + \theta_t) \right] - \theta_t, \quad (28)$$

where

$$\theta_t = \arctan \left\{ \frac{\sin(\theta_{l, f_i})}{n - \cos(\theta_{l, f_i})} \right\}. \quad (29)$$

However, if the direction of original divergent angle meets the principle of wave path consistency, the l th mode OAM beam still maintains the characteristics of the l th mode OAM beams after passing through the lens. Specifically, if wave path is equal to $m\lambda$, where m is a positive integer, the phase of beams remains unchanged. Therefore, we need to make sure that the difference of wave path between the internal lens and the single focal lens equals to $m\lambda$.

According to Fig. 5, the wave path emitted from the focal f_e , denote by $L(f_e)$, is given as follows:

$$L(f_e) = \frac{f_e}{\cos \theta_l} + \frac{nT_{\max}}{\cos \tau}, \quad (30)$$

where T_{\max} is maximum thickness of the internal lens, and $T_{\max}/\cos\tau$ is the thickness that beams pass through the internal lens. On contrast, as the focal distance of lens is f_i , the beam that emitted from the focal f_i has no divergent angle after passing through the lens. Therefore, the wave path emitted from focal f_i , denote by $L(f_i)$, is given as follows:

$$L(f_i) = \frac{f_i}{\cos(\theta_{l,f_i})} + nT_{\max}, \quad (31)$$

where θ_{l,f_i} is the divergent angle of OAM beams when the focal distance is f_i .

If the difference between $L(f_i)$ and $L(f_e)$ is equal to $m\lambda$, the wavefront of beams that emitted from focal f_e remains unchanged after passing through the internal lens. Because the internal lens is very thin, in order to simplify the calculation, $\frac{nt_{\max}}{\cos\tau}$ can be approximate to nt_{\max} . Thus, the simplified relationship between f_i and f_e is given as follows:

$$m\lambda + \frac{f_e}{\cos\theta_l} = \frac{f_i}{\cos(\theta_{l,f_i})}. \quad (32)$$

Combining $f_i \tan(\theta_{l,f_i}) = f_e \tan\theta_l$ and Eq. (32), f_i that maintaining the wavefront of OAM beams is obtained as follows:

$$f_i = \sqrt{\left(m\lambda + \frac{f_e}{\cos\theta_l}\right) f_e \tan\theta_l}. \quad (33)$$

The downgrading caused by lens on OAM beams of high-order OAM-mode are relatively small. To simply the design of bifocal lens, we only make the internal lens cover the range of 1th mode OAM beams. Substituting Eq. (27) into Eq. (33), ρ can be written as follows:

$$\rho = \frac{\sqrt{\left(m\lambda + \frac{f_e}{\cos\theta_l}\right) f_e \tan\theta_l}}{f_e}. \quad (34)$$

In order to better analyze the bifocal lens, we give the amplitude of OAM beams after passing through the bifocal lens. Based on the amplitude of beams after passing through the single focal lens in Eq. (22), a longer focal distance of the internal lens makes the lens thinner in the center, while a thinner lens reduces the downgrading of OAM beams. When the divergent angle of OAM beams is smaller than ν , the beams pass through the internal lens. Otherwise, the beams pass through the external lens. Thus, the amplitude of OAM beams after passing through the bifocal lens is given as follows:

$$A_B(r, \theta) = \begin{cases} A_L(r, f_i) & \theta < \nu; \\ A_L(r, f_e) & \theta > \nu. \end{cases} \quad (35)$$

With the amplitude of beams after passing through the bifocal lens of the single focal lens, we can prove that our designs significantly increase the SE of wireless communications. To evaluate our developed lens and bifocal lens, we are going to give the capacity of OAM based radio vortex wireless communications in the next section.

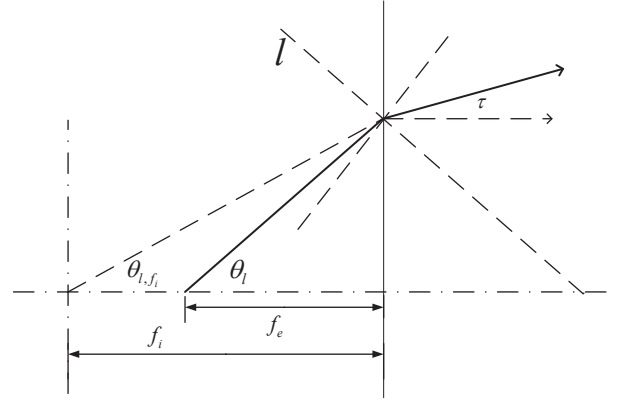


Fig. 5. Refraction path of internal lens.

B. The Capacity of bifocal lens OAM Based Radio Vortex Wireless Communications

The bifocal lens can mitigate the SNR downgrading caused by lens. According to Eq. (35), SNR of bifocal lens based radio vortex wireless communication using converged OAM with the index l , denoted by SNR_l'' , can be written as follows:

$$\text{SNR}_l'' = \frac{A_B(r, \theta) A_{er}}{(4\pi d)^2 N_0} P_t. \quad (36)$$

When the beam of the l th OAM-mode passes through the internal lens, the internal lens impacts the amplitude of beams, that is $\theta < \nu$, $A_B(r, \theta) = A_L(r, f_i)$. On the other hand, when the beam of the l th OAM-mode passes through the external lens, the amplitude of beam is impacted by the external lens, that is $\theta > \nu$, $A_B(r, \theta) = A_L(r, f_e)$. Thus, the capacity of radio vortex wireless communication using OAM beams converged by the bifocal lens, denoted by C_B , is expressed in Eq. (37).

After converging by the lens antenna, OAM beams are converged into cylinder-like beams. When the propagation distance is short, main lobes of both converged and diverged beams can be received by antenna. When the propagation distance is long enough, the divergent OAM beams cannot be received by antenna. The converged OAM beams can be received within a relatively long distance. Thus, the converged OAM beams with multiple OAM-modes can be used in a relatively long range to increase the spectrum efficiency of wireless communication.

VI. SIMULATION AND EVALUATION

In this section, we evaluate the performance of our proposed lens antenna and bifocal lens antenna designs, where HFSS [25] is used to simulate and verify our designs. Moreover, the obtained capacity is verified. We set $f_r = 35$ GHz and $\epsilon_r = 2.2$. The parameters of UCA are calculated according to Eqs. (38)-(41) and we have $W_P = 3.388$ mm, $L_P = 2.947$ mm, $\Delta L = 0.438$ mm, and $\epsilon_{re} = 2.039$.

According to the relationship between θ and R mentioned before, we choose to use 16 patch elements UCA in the following simulation by trading off the size of UCA and the

$$C_B = \sum_{l=1}^L B \log_2(1 + \text{SNR}_l'') = \begin{cases} \sum_{l=1}^L B \log_2 \left\{ 1 + \frac{[G_t'(l) \frac{a(n \cos \varphi - 1)^3}{f_e^2(n-1)^2(n-\cos \varphi)} - pT(f_i, \theta_l)] \lambda^2 G_0}{(4\pi d)^2 N_0} P_t \right\} & \theta < \nu; \\ \sum_{l=1}^L B \log_2 \left\{ 1 + \frac{[G_t'(l) \frac{a(n \cos \varphi - 1)^3}{f_e^2(n-1)^2(n-\cos \varphi)} - pT(f_e, \theta_l)] \lambda^2 G_0}{(4\pi d)^2 N_0} P_t \right\} & \theta > \nu. \end{cases} \quad (37)$$

divergent angle of OAM beams. We select $f_e = 30$ mm, $m = 1.67$, $R = 0.6\lambda$ and $\rho = 2.17$. Thus, we have $f_i = 65.3$ mm and $r = 25$ mm, which can be obtained using Eq. (27).

Figures 6 and 7 depict the E field of OAM beams observing from the horizontal direction and vertical direction, respectively. It can be seen from Fig. 6 that the divergent angle of OAM beam increases as the index of OAM-mode increases. When the propagation distance is very large, OAM beams of high-order OAM-mode diverge to be centrally hollow, which makes the radio vortex signal very difficult to be received. After converging by the bifocal lens antenna, the divergent degree of OAM beams is significantly reduced. Observing Fig. 6, we can find that OAM beams are nearly converged into columnar beams, where we place the plane at 100 mm to observe the results. The external lens does not cover the divergent angle of the side lobes. Thus, the side lobes of high-order OAM beams doesn't impact the transmission. For the plane beam, the gain of side lobes is downgraded due to very large power attenuation in the center of lens antenna. As shown in Fig. 7, the E field of divergent OAM beams cannot be detected while the converged OAM beams can be easily detected on the height of 100 mm above the UCA. We can also see that the convergent OAM beams still have the vortex wavefront characteristics, which confirms that lens antennas do not violate the wavefront characteristics of OAM beams.

Figure 8 shows the 2D radiation pattern of original PE beams, lens converged PE beams, and bifocal focal lens converged PE beams. Adjacent OAM-modes have too much overlapped area with each other, which makes receivers very hard to separate them. Thus, we choose to simultaneously generate PE beam and vortex beams with OAM-mode 2 and 4, which satisfies the requirement of multiple independent data traffic transmissions. As shown in Fig. 8, the gain of plane beam converged by lens antenna is severely reduced. To solve this problem, we reduce the thickness of the center of lens antenna. According to the simulation results, the downgrading is very small for the convergent plane beam when using the bifocal lens antenna.

Figure 9 shows the capacities of OAM beams based wireless communication. As shown in Fig. 9, the capacity of convergent OAM beam based radio vortex wireless communication using bifocal lens is larger than that of the divergent OAM beam based radio vortex wireless communication. For the radio vortex communication using OAM-mode 1, the capacity of divergent OAM based radio vortex wireless communication is very close to the capacity of converged OAM based ra-

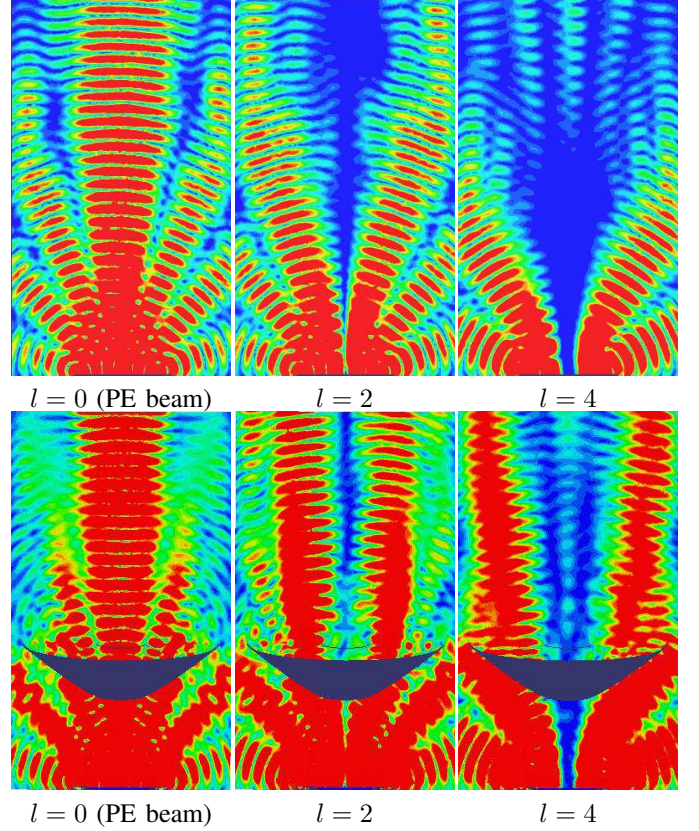


Fig. 6. E field of OAM beams (horizontal direction).

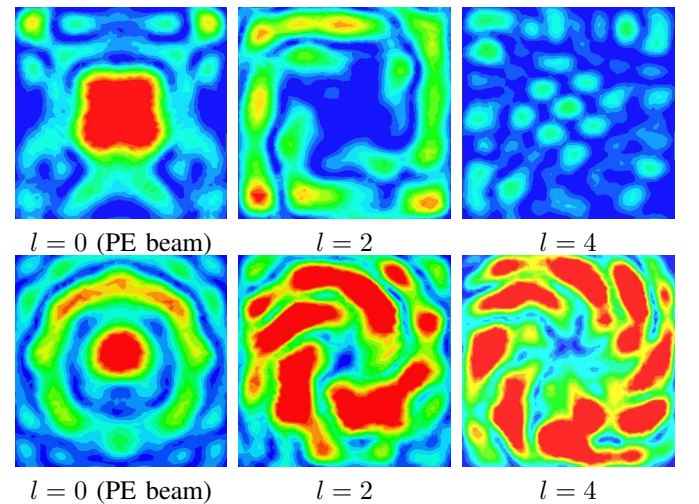


Fig. 7. E field of OAM beams (vertical direction).

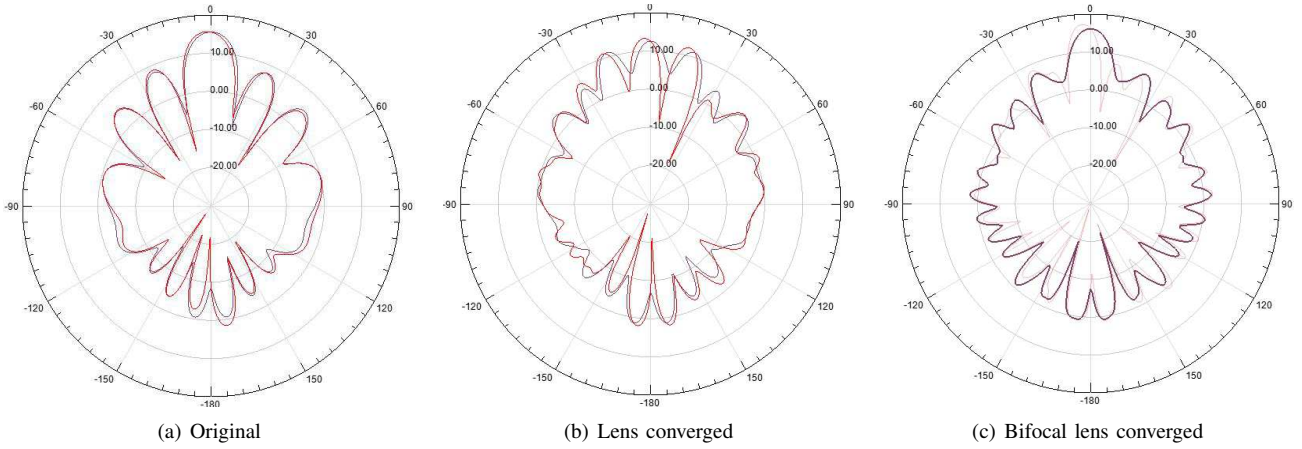


Fig. 8. 2D radiation pattern of original PE beams, lens converged PE beams, and bifocal focal lens converged PE beams.

dio vortex wireless communication. This result shows that the bifocal lens does not downgrade the beams too much while the convergence makes the power more concentrated. Moreover, the advantage of convergent OAM based radio vortex communication significantly increases as the number of OAM-mode increases. For the divergent OAM based radio vortex communication, the incremental of capacity reduces as the OAM-mode increase because the high-order OAM-mode can be received with low power. Although the lens causes somewhat SNR downgrading, the convergence makes the power more concentrated. Thus, the capacity of convergent OAM beam based radio vortex wireless communication is significantly increased.

Figure 10 shows the capacities of OAM beams based wireless communication taking into account the focal distance of lens antenna. The focal distance and diameter impact the thickness of lens. When the diameter of lens remains unchanged, the lens becomes thinner as the focal distance increases. However, in our lens design, in order to converge multiple OAM beams, the lens should be able to cover the maximum divergent angle of OAM beams. The diameter of lens is in associate with the focal distance. The thickness of lens grows as focal distance increases, thus causing a severe downgrading for OAM beams. Therefore, the capacity decreases as focal distance increases. In addition, the divergent angles of OAM beams with different OAM-modes are different. Table. I shows that the divergent angle increases as OAM-mode increases. The center of lens is thicker, causing greater downgrading. It can be also seen from Fig. 10 that when $f = 40$ mm, the capacity of OAM-mode 0 is very close to zero. This is because the received SNR is very close to zero given the fixed reception area.

Figure 11 shows the capacities of OAM beams based wireless communication with different radius of UCA. The maximum divergent angle increases with the radius decreases. The diameter of lens increase as the increase of radius. Thus, The center of lens is thinner, reducing the SNR downgrading. We can conclude from Fig 11 that the capacity of OAM beams

based wireless communication increases as the increase of radius of UCA. However, as the radius becomes bigger, the capacity grows at a decreasing rate. Thus, for the sake of the strength of OAM beams, the radius should be selected in the middle range. In addition, according to our simulation, a in Eq. (22) is about 10^{-3} . Thus, the SNR downgrading caused by lens has a much greater effect than the energy redistribution of lens.

VII. CONCLUSIONS

In this paper, we proposed the UCA and lens based antennas to converge OAM beams of multiple OAM-modes. We obtained that multiple OAM beams generated by UCA antenna can be converged by lens antennas, while the wavefront property of OAM beams can be maintained. Moreover, our proposed bifocal lens can significantly decrease the downgrading on the strength of PE beam and OAM beams with low-order OAM-mode. We proved that after converging, the capacity of radio vortex wireless communications can be significantly increased. In addition, we give the relationship between the divergent angle of OAM beams and the radius of UCA antenna, which provides the guidance for the design of UCA antenna.

APPENDIX

1) *Design of UCA Antenna:* We design the patch based UCA antenna. The profile of a 16 patch elements based UCA is shown in Fig. 2, where patch elements are equally distributed around the circle. To achieve the best feed performance, it is needed to design the size of patch elements [23]. The width of the patch, denoted by W_P , is given as follows [32], [33]:

$$W_P = \frac{c}{2f_r} \left(\frac{\varepsilon_r + 1}{2} \right)^{-1/2}, \quad (38)$$

where c represents the speed of light in vacuum, ε_r is relative permittivity, and f_r is the operating frequency of antenna.

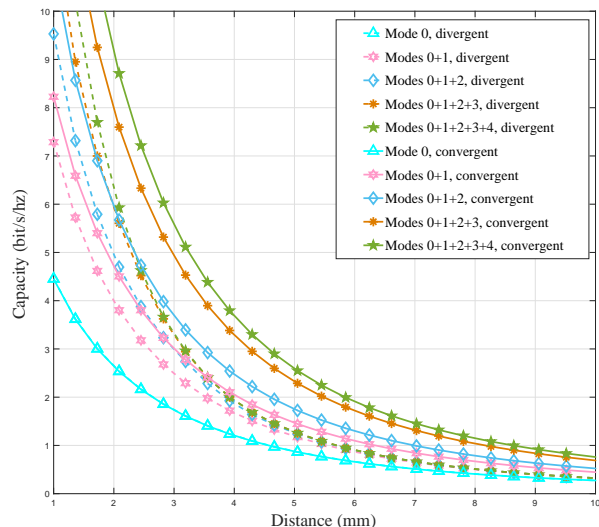


Fig. 9. Capacities of OAM beams based communication.

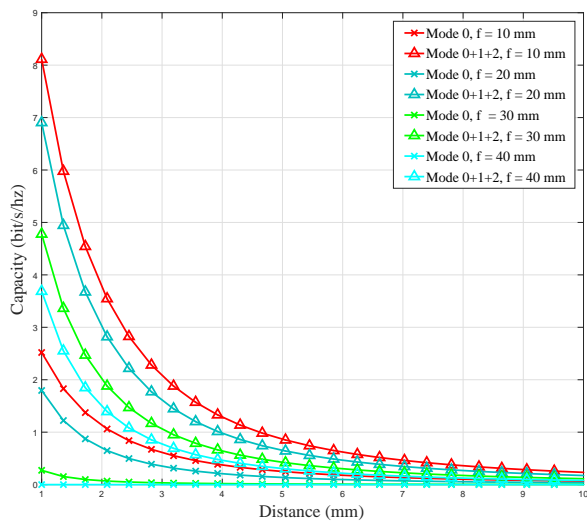


Fig. 10. Capacities of OAM beams based communication versus focal distance with focal lens.

Then, we can obtain the relative effective permittivity of the dielectric substrate, denoted by ϵ_{re} , as follows:

$$\epsilon_{re} = \frac{\epsilon_{re} + 1}{2} + \frac{\epsilon_{re} - 1}{2} \left(1 + \frac{10h}{W_P} \right)^{-1/2}, \quad (39)$$

where h is the thickness of dielectric substrate.

The patch element edge field results in the equivalent length of radiation gap (stretching effects) [32], denoted by ΔL , which is expressed as follows:

$$\Delta L = 0.412h \frac{(\epsilon_{re} + 0.3)(W_P/h + 0.264)}{(\epsilon_{re} - 0.258)(W_P/h + 0.8)}. \quad (40)$$

Theoretically, the length of patch element, denoted by L_P , should be half of the effective wavelength. However, due to

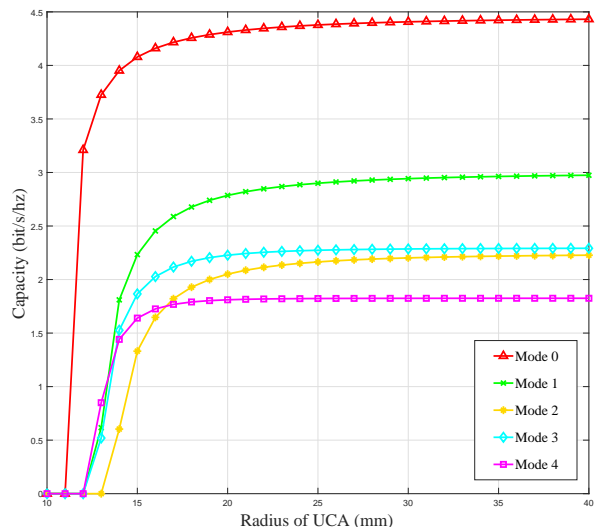


Fig. 11. Capacities of OAM beams based communication with different radius of UCA.

the stretching effects of the field, the stretching length ΔL needs to be removed from the patch element's length L_P . Thus, we have:

$$L_P = \frac{\lambda_g}{2} - 2\Delta L = \frac{c}{2f_r \sqrt{\epsilon_{re}}} - 2\Delta L, \quad (41)$$

where λ_g is the effective wavelength [34].

REFERENCES

- [1] S. Gao, W. Cheng, H. Zhang, and Z. Li, "High-efficient beam-converging for UCA based radio vortex wireless communications," in *IEEE ICC 2017*, Qingdao, Oct. 2017, pp. 1–7.
- [2] J. G. Andrews, S. Buzzi, W. Choi, S. V. Hanly, A. Lozano, A. C. K. Soong, and J. C. Zhang, "What will 5G be?," *IEEE Journal on Selected Areas in Communications*, vol. 32, no. 6, pp. 1065–1082, June 2014.
- [3] X. Zhang, W. Cheng, and H. Zhang, "Full-duplex transmission in phy and mac layers for 5g mobile wireless networks," *IEEE Wireless Communications*, vol. 22, no. 5, pp. 112–121, October 2015.
- [4] W. Cheng, W. Zhang, H. Jing, S. Gao, and H. Zhang, "Orbital angular momentum for wireless communications," *IEEE Wireless Commun. Mag.*, to be published, 2018.
- [5] L. Liang, W. Cheng, H. Zhang, Z. Li, and Y. Li, "Orbital-angular-momentum based mode-hopping: A novel anti-jamming technique," in *IEEE ICC 2017*, Qingdao, Oct. 2017, pp. 1–7.
- [6] Y. Yang, W. Cheng, W. Zhang, and H. Zhang, "Mode modulation for orbital-angular-momentum based wireless vorticose communications," in *IEEE GLOBECOM 2017*, Singapore, Dec. 2017, pp. 1–7.
- [7] B. Thidé, H. Then, J. Sjöholm, K. Palmer, J. Bergman, T. D. Carozzi, Y. N. Istomin, N. H. Ibragimov, and R. Khramitova, "Utilization of photon orbital angular momentum in the low-frequency radio domain," *Physical Review Letters*, vol. 99, no. 8, pp. 087701, 2007.
- [8] W. Cheng, H. Zhang, L. Liang, H. Jing, and Z. Li, "Orbital-angular-momentum embedded massive mimo: Achieving multiplicative spectrum-efficiency for mmwave communications," *IEEE Access*, vol. 6, pp. 2732–2745, 2018.
- [9] A. Bennis, R. Niemic, C. Brousseau, K. Mahdjoubi, and O. Emile, "Flat plate for OAM generation in the millimeter band," in *European Conference on Antennas and Propagation*, 2013, pp. 3203–3207.
- [10] R. Niemic, C. Brousseau, K. Mahdjoubi, O. Emile, and A. Ménard, "Characterization of an OAM Flat-Plate Antenna in the Millimeter Frequency Band," *IEEE Antennas and Wireless Propagation Letters*, vol. 13, pp. 1011–1014, 2014.

- [11] X. Hui, S. Zheng, Y. Hu, C. Xu, X. Jin, H. Chi, and X. Zhang, "Ultralow reflectivity spiral phase plate for generation of millimeter-wave OAM beam," *IEEE Antennas and Wireless Propagation Letters*, vol. 14, pp. 966–969, 2015.
- [12] W. J. Byun, Y. S. Lee, B. S. Kim, K. S. Kim, M. S. Kang, and Y. H. Cho, "Simple generation of orbital angular momentum modes with azimuthally deformed Cassegrain subreflector," *Electronics Letters*, vol. 51, no. 19, pp. 1480–1482, 2015.
- [13] C. Deng, W. Chen, Z. Zhang, Y. Li, and Z. Feng, "Generation of OAM radio waves using circular vivaldi antenna array," *International Journal of Antennas and Propagation*, 2013, (2013-5-7), vol. 2013, no. 2, pp. 607–610, 2013.
- [14] Q. Bai, A. Tennant, B. Allen, and M. U. Rehman, "Generation of orbital angular momentum (OAM) radio beams with phased patch array," in *2013 Loughborough Antennas Propagation Conference (LAPC)*, Nov 2013, pp. 410–413.
- [15] X. Ge, R. Zi, X. Xiong, Q. Li, and L. Wang, "Millimeter wave communications with OAM-SM scheme for future mobile networks," *IEEE Journal on Selected Areas in Communications*, vol. 35, no. 9, pp. 2163–2177, Sept 2017.
- [16] Y. Ren, L. Li, G. Xie, Y. Yan, Y. Cao, H. Huang, N. Ahmed, Z. Zhao, P. Liao, C. Zhang, G. Caire, A. F. Molisch, M. Tur, and A. E. Willner, "Line-of-sight millimeter-wave communications using orbital angular momentum multiplexing combined with conventional spatial multiplexing," *IEEE Transactions on Wireless Communications*, vol. 16, no. 5, pp. 3151–3161, May 2017.
- [17] W. Wei, K. Mahdjoubi, C. Brousseau, and O. Emile, "Generation of OAM waves with circular phase shifter and array of patch antennas," *Electronics Letters*, vol. 51, no. 6, pp. 442–443, 2015.
- [18] S. M. Mohammadi, L. K. S. Daldorff, J. E. S. Bergman, R. L. Karlsson, B. Thidé, K. Forozesh, T. D. Carozzi, and B. Isham, "Orbital angular momentum in radio; a system study," *IEEE Transactions on Antennas and Propagation*, vol. 58, no. 2, pp. 565–572, Feb 2010.
- [19] F. E. Mahmoudi and S. D. Walker, "4-Gbps uncompressed video transmission over a 60-GHz orbital angular momentum wireless channel," *IEEE Wireless Communications Letters*, vol. 2, no. 2, pp. 223–226, April 2013.
- [20] Y. Chen, S. Zheng, Y. Li, X. Hui, X. Jin, H. Chi, and X. Zhang, "A flat-lensed spiral phase plate based on phase-shifting surface for generation of millimeter-wave OAM beam," *IEEE Antennas and Wireless Propagation Letters*, vol. 15, pp. 1156–1158, 2016.
- [21] N. Kou, S. Yu, and L. Li, "Generation of high-order Bessel vortex beam carrying orbital angular momentum using multilayer amplitude-phase-modulated surfaces in radiofrequency domain," *Applied Physics Express*, vol. 10, no. 1, pp. 016701, 2017.
- [22] R. C. Johnson and H. Jasik, *Antenna engineering handbook /2nd edition/*, 1984.
- [23] T. A. Milligan, *Modern antenna design*, McGraw-Hill, 1985.
- [24] J. Sjöholm and P. Kristoffer, "Angular momentum of electromagnetic radiation. fundamental physics applied to the radio domain for innovative studies of space and development of new concepts in wireless communications," *Physics*, vol. 48, no. 1, pp. 15–21, 2009.
- [25] HFSS ANSYS, "Ansoft corp., pittsburgh, pa," 2015.
- [26] J. Kraus and R. Marhefka, *Antennas for all applications*, McGraw-Hill, 2003.
- [27] T. S. Rappaport, *Wireless communications: principles and practice.*, New Jersey: prentice hall PTR, 1996.
- [28] S. Samuel, *Microwave antenna theory and design*, P. Peregrinus on behalf of the Institution of Electrical Engineers., 1984.
- [29] R. Johnson, "Antenna engineering handbook," 1961.
- [30] C. Clapp, C. J. Koester, and A. Vander, "Optical and electro-optical information processing," vol. 30, no. 4, pp. 308–322, 1965.
- [31] C. A. Fernandes and J. G. Fernandes, "Performance of lens antennas in wireless indoor millimeter-wave applications," *IEEE Transactions on Microwave Theory and Techniques*, vol. 47, no. 6, pp. 732–737, June 1999.
- [32] I. J. Bahl and P. Bhartia, *Microstrip antennas*, Artech House, 1980.
- [33] I. Bahl, P. Bhartia, and S. Stuchly, "Design of microstrip antennas covered with a dielectric layer," *IEEE Transactions on Antennas and Propagation*, vol. 30, no. 2, pp. 314–318, 1982.
- [34] R. D. Javor, X. Wu, and K. Chang, "Design and performance of a microstrip reflectarray antenna," *IEEE Transactions on Antennas and Propagation*, vol. 43, no. 9, pp. 932–939, Sep 1995.